
SOLVING TIME-DEPENDENT PARAMETRIC PDES BY MULTICLASS CLASSIFICATION-BASED REDUCED ORDER MODEL

Chen Cui[‡], Kai Jiang[†] and Shi Shu[‡]

¹School of Mathematics and Computational Science, Hunan Key Laboratory for Computation and Simulation in Science and Engineering, Xiangtan University, Xiangtan, Hunan, 411105, China.

November 12, 2021

ABSTRACT

In this paper, we propose a network model, the multiclass classification-based ROM (MC-ROM), for solving time-dependent parametric partial differential equations (PPDEs). This work is inspired by the observation of applying the deep learning-based reduced order model (DL-ROM) [1] to solve diffusion-dominant PPDEs. We find that the DL-ROM has a good approximation for some special model parameters, but it cannot approximate the drastic changes of the solution as time evolves. Based on this fact, we classify the dataset according to the magnitude of the solutions, and construct corresponding subnets dependent on different types of data. Then we train a classifier to integrate different subnets together to obtain the MC-ROM. When subsets have the same architecture, we can use transfer learning technology to accelerate the offline training. Numerical experiments show that the MC-ROM improves the generalization ability of the DL-ROM both for diffusion- and convection-dominant problems, and maintains the DL-ROM's advantage of good approximation ability. We also compare the approximation accuracy and computational efficiency of the proper orthogonal decomposition (POD) which is not suitable for convection-dominant problems. For diffusion-dominant problems, the MC-ROM can save about 100 times online computational cost than the POD with a slightly better approximation in the reduced space of the same dimension.

Keywords Parametrized partial differential equation, Reduced order model, Deep learning, Generalization ability, Classification, Computational complexity.

1 Introduction

Partial differential equation (PDE) is a fundamental mathematical model in scientific and engineering computation. It is urgent to develop a numerical approach for solving PDEs. The approach requires the following properties: high fidelity, generalization ability (being available to different PDE, different initial-boundary condition, model parameters, and so on), computational efficiency (being expected to achieve the optimal $O(N)$ computational complexity). The approach is in terms of computational PDE model. Parametric PDEs (PPDEs) are one of the most important PDEs. Many scientific and engineering problems, such as control, optimization, inverse design, uncertainty quantification, Bayesian inference can be described by PPDEs with computational domains, initial-boundary conditions, source terms, and physical properties as parameters. However, numerically solving PPDEs usually requires expensive computational costs mainly due to multi-query and real-time computing. Therefore, designing a computational PDE model that meets the above characteristics for the PPDEs has important applications. However, it is also a challenging in scientific and engineering computation.

* cuichensx@gmail.com

[†] kaijiang@xtu.edu.cn

[‡] shushi@xtu.edu.cn

Projection-based linear reduced order model (ROM) [2, 3] is an effective way to improve the computational efficiency of numerically solving PPDEs. ROM can be divided into offline and online stages. The offline stage constructs a low-dimensional subspace to approximate the solution manifold using obtained high fidelity numerical solutions. The computational tasks on the offline stage are usually expensive. The online stage obtains an approximated solution for a new given model parameter based on the low-dimensional subspace. Proper orthogonal decomposition (POD) method is a popular algorithm for constructing linear ROM and is effective for many questions, such as computational fluid dynamics and structural analysis [4, 5]. However, the POD method still has some weaknesses, such as (i) it requires to construct a relatively high-dimensional subspace to obtain an acceptable numerical solution; (ii) it needs relatively expensive reduction strategies; and (iii) it has the intrinsic difficulty to handle physical complexity, etc. To overcome these difficulties, a non-intrusive and data-driven nonlinear reduced-order model based on deep learning (or neural network) has been developed [6, 7].

Using the neural network as an ansatz to solve PDE can be traced back to the late 1990s [8]. In recent years, with the evolution of the computational power, the explosive development of deep learning has again attracted much attention of the community of scientific computing. Due to the great expressivity of neural network [9], the neural-network PDE solver achieves some breakthroughs in solving a single PDE, especially high-dimensional PDE [10, 11, 12]. Using neural networks to solve PPDEs has also been attracted much attention. The idea is applying neural networks to learn the parameter to solution mapping. The main works can be divided into two parts based on the steady-state and time-dependent PPDEs. Firstly, the works on steady-state PPDEs can be divided into supervised learning [13, 14] and unsupervised learning [15, 16]. Secondly, since time-dependent PPDEs also involve time variables, the requirements for its generalization ability are also stronger. Solving time-dependent PPDEs using deep learning can be mainly divided into two perspectives: continuous and discretization. Under continuous perspective, the input and output spaces are both infinite-dimensional, then the corresponding mapping is an operator between infinite-dimensional spaces. Refs [17, 18, 19, 20] give the corresponding algorithms. Refs [21, 22] introduce dimension reduction technologies to transform it into a certain finite-dimensional problem. From a discretization perspective, the authors extract the characteristic parameters of the PDE model, which can be denoted as $\mu = [\mu_1, \dots, \mu_{n_\mu}] \in \mathcal{P}$, \mathcal{P} is compact in \mathbb{R}^{n_μ} , then design the corresponding network architecture according to the characteristics of different problems. Refs [23, 24, 25] firstly reduce the dimension of the solution manifold, and then use LSTM or NeuralODE to evolve low-dimensional system to obtain the solutions at each time layer, respectively. Refs [26] develop a network model with spatiotemporal variables as input parameters, which overcomes the curse of dimensionality. Fresca et al. [1] designed a nonlinear ROM based on convolutional autoencoder, which is called deep learning-based reduced order model (DL-ROM), and use it to solve some nonlinear time-dependent PDEs. DL-ROM can predict the numerical solution of the corresponding PPDEs on spatial discretization points for any given (μ, t) . However, the generalization ability of DL-ROM when dealing with diffusion-dominant problems becomes weak. Designing an effective network that satisfies the properties of the computational PDE model for solving PPDEs is the concern of this article.

In this work, we firstly repeat numerical experiments of one-dimensional (1D) viscous Burgers equation in [1] by the DL-ROM. We find that when the order of magnitude of the solution changes drastically as time evolves, DL-ROM cannot capture the drastic changes of the solution. Based on this observation, we propose a multiclass classification-based reduced order model (MC-ROM) for solving time-dependent PPDEs. MC-ROM classifies the training data according to the magnitude of the numerical solution and build different subnets for each type of data. When subsets have the same architecture, we can use transfer learning techniques to accelerate offline training. Finally, in order to bring a new parameter into the corresponding subnet in the testing stage, we assign labels to the training data and train a classifier based on these data by support vector machine (SVM). MC-ROM is composed of the classifier and these subnets. We also point out that the choice of subnet depends on the problem. This paper chooses DL-ROM as the subnet because of its good approximation ability for convection problems and efficient online calculation. Numerical experiments show that MC-ROM has sufficient generalization ability for both diffusion- and convection-dominant problems and has the following advantages: (i) MC-ROM can approximate the equation includes some terms that can lead to rapid variation in the solution with acceptable accuracy, while DL-ROM cannot. (ii) MC-ROM is very efficient compared with POD in online computation. We analyze the online computational complexity of MC-ROM and POD, and both are $O(N)$ for parameter separable problems. However, the latter is much more expensive for other types of equations. In our experiments, MC-ROM is about 100 times faster than POD when solving a two-dimensional (2D) parabolic equation with discontinuous coefficients. Moreover, POD is not suitable for convection-dominant problems. (iii) MC-ROM can be easily extended and improved. Once a new model that approximates the solution mapping is proposed, we can use it as a subnet to improve the approximation of MC-ROM.

The rest of this paper is organized as follows. Section 2 formulates the problem and introduces the corresponding numerical methods. Section 3 introduces the ROM, including POD and DL-ROM. Section 4 finds that when the equation is diffusion-dominated, DL-ROM's generalization ability has troubles, and we give an explanation. Based on this observation, in Section 5 we propose the MC-ROM and analyze its online calculation complexity. In Section 6,

we apply the MC-ROM to solve the 1D viscous Burgers equation and the 2D parabolic equation. The approximation accuracy and calculation time of solving these equations are compared with DL-ROM and with POD. Finally, Section 7 summarizes and discusses.

2 Problem definition

Consider the following time-dependent PPDE

$$\dot{u}(\mathbf{x}, t, \boldsymbol{\mu}) + \mathcal{N}[u(\mathbf{x}, t, \boldsymbol{\mu})] + \mathcal{L}[u(\mathbf{x}, t, \boldsymbol{\mu}); \boldsymbol{\mu}] = 0, \quad (\mathbf{x}, t, \boldsymbol{\mu}) \in \Omega \times \mathcal{T} \times \mathcal{P}, \quad (2.1)$$

where \dot{u} is the derivative of u with respect to t , $\Omega \subset \mathbb{R}^d$ is a bounded open set, $\mathcal{T} = [0, T]$, parameter space $\mathcal{P} \subset \mathbb{R}^{n_\mu}$ is compact, and \mathcal{N}, \mathcal{L} are nonlinear and linear operator respectively. This equation (2.1) is well-defined with appropriate initial and boundary conditions.

Use spatial discretization methods such as finite element method (FEM) and finite difference method (FDM) to discretize equations (2.1), we obtain the following ODE system

$$\dot{\mathbf{u}}_h(t, \boldsymbol{\mu}) = \mathbf{f}(\mathbf{u}_h, t; \boldsymbol{\mu}) \quad (t, \boldsymbol{\mu}) \in \mathcal{T} \times \mathcal{P}, \quad (2.2)$$

where $\mathbf{u}_h : \mathcal{T} \times \mathcal{P} \rightarrow \mathbb{R}^{N_h}$, N_h is the spatial degrees of freedom.

Next, for time discretization, \mathcal{T} is uniformly divided into N_t segments, $\{t^k\}_{k=1}^{N_t}$ are time layers to be solved, where $t^k = k\Delta t$, $\Delta t = T/N_t$. We apply linear multi-step method to solve (2.2), which becomes a fully discretized system

$$\mathbf{r}^k(\mathbf{u}_h^k; \boldsymbol{\mu}) = \mathbf{0}, \quad k = 1, \dots, N_t, \quad (2.3)$$

the discrete residual of the k th time layer $\mathbf{r}^k : \mathbb{R}^{N_h} \times \mathcal{P} \rightarrow \mathbb{R}^{N_h}$ is defined as

$$\mathbf{r}^k : (\boldsymbol{\xi}; \boldsymbol{\mu}) \mapsto \alpha_0 \boldsymbol{\xi} - \Delta t \beta_0 \mathbf{f}(\boldsymbol{\xi}, t^k; \boldsymbol{\mu}) + \sum_{j=1}^K \alpha_j \mathbf{u}_h^{kj} - \Delta t \sum_{j=1}^K \beta_j \mathbf{f}(\mathbf{u}_h^{kj}, t^{kj}; \boldsymbol{\mu}). \quad (2.4)$$

Coefficients $\alpha_j, \beta_j, j = 0, \dots, K$ with $\sum_{j=0}^K \alpha_j = 0$ determine a concrete linear multi-step method. Expressions (2.2)-(2.4) are full order model (FOM) of PDE (2.1).

Given a parameter $\boldsymbol{\mu} \in \mathcal{P}$, its corresponding PDE (2.1) is solved by FOM. When the spatial discrete degree of freedom N_h is large, the obtained algebraic system is large-scale. Solving such a large system is expensive. Moreover, when $\boldsymbol{\mu}$ changes, FOM is required to repeat the above expressions (2.2)-(2.4), which increases the computational cost again. How to solve these problems is the focal point of this paper.

3 Reduced order model

From the previous section we saw when N_h is large, the equation (2.3) is large-scale. However, the inherent dimension of solution manifold $\mathcal{S}_h = \{\mathbf{u}_h(t; \boldsymbol{\mu}) \mid t \in [0, T] \text{ and } \boldsymbol{\mu} \in \mathcal{P} \subset \mathbb{R}^{n_\mu}\}$ usually not exceed the dimension of parameter space [27, 28]. Hence we can use the solution on the low-dimensional manifold to accurately represent the FOM solution $\mathbf{u}_h(t; \boldsymbol{\mu})$. Based on this hypothesis, ROM was proposed. In this section we introduce a commonly used linear ROM and a nonlinear ROM.

3.1 Projection based ROM

Let $n \ll N_h$, $\mathbf{u}_n(t; \boldsymbol{\mu}) \in \mathbb{R}^n$ be the dimension and numerical solution of low-dimensional space, respectively. $V \in \mathbb{R}^{N_h \times n}$ is a linear lifting operator, $\text{Col}(V)$ represents the linear space spanned by the column vector of V . Linear ROM pursuits an approximation on a n -dimensional trial manifold $\mathcal{S}_n = \text{Col}(V)$, the approximation of FOM solution \mathbf{u}_h can be obtained by a decoder V , denoted as \mathbf{h}_{dec}

$$\mathbf{u}_h(t; \boldsymbol{\mu}) \approx \tilde{\mathbf{u}}_h(t; \boldsymbol{\mu}) = V \mathbf{u}_n(t; \boldsymbol{\mu}). \quad (3.1)$$

POD is one of the most widely used method to generate such a linear trial manifold. It corresponds to the principal component analysis (PCA) in data science. The difference between POD and PCA is that the former retains the reduced system and the latter does not. In the following, we will briefly introduce POD. More details can refer to [4, 27, 28].

Step 1: Data collection. Sample N_{train} parameters in the parameter space in a certain distribution, numerically solving the corresponding PDE (2.3), and assemble them into a snapshot matrix $S \in \mathbb{R}^{N_h \times N_s}$

$$S = [\mathbf{u}_h(t^1; \boldsymbol{\mu}_1) \dots \mathbf{u}_h(t^{N_t}; \boldsymbol{\mu}_{N_t})], i = 1 \dots N_{train}, \quad (3.2)$$

here $N_s = N_{train} N_t$.

Step 2: Computing singular value decomposition (SVD) of S

$$S = U \Sigma Z^T, \quad (3.3)$$

where $U = [\zeta_1, \dots, \zeta_{N_h}] \in \mathbb{R}^{N_h \times N_h}$, $Z = [\psi_1, \dots, \psi_{N_s}] \in \mathbb{R}^{N_s \times N_s}$ are both orthogonal, $\Sigma = \text{diag}(\sigma_1, \dots, \sigma_r) \in \mathbb{R}^{N_h \times N_s}$, singular value $\sigma_1 \geq \sigma_2 \geq \dots \geq \sigma_r > 0$, $r \leq \min(N_h, N_s)$. Take the first n left singular vectors of S as $V = [\zeta_1, \dots, \zeta_n]$.

Step 3: Generate reduced system. Substituting $V \mathbf{u}_n(t; \boldsymbol{\mu})$ into the ODE system (2.2) we get

$$V \dot{\mathbf{u}}_n(t; \boldsymbol{\mu}) = \mathbf{f}(V \mathbf{u}_n(t; \boldsymbol{\mu}), t; \boldsymbol{\mu}) \quad (t, \boldsymbol{\mu}) \in \mathcal{T} \times \mathcal{P}. \quad (3.4)$$

Let the residuals be orthogonal to $\text{Col}(V)$, we obtain the reduced system

$$V^T V \dot{\mathbf{u}}_n(t; \boldsymbol{\mu}) = V^T \mathbf{f}(V \mathbf{u}_n(t; \boldsymbol{\mu}), t; \boldsymbol{\mu}) \quad (t, \boldsymbol{\mu}) \in \mathcal{T} \times \mathcal{P}. \quad (3.5)$$

The POD method introduced above is a Galerkin method. More generally, let $W \in \mathbb{R}^{N_h \times n}$, $W \neq V$ and

$$W^T V \dot{\mathbf{u}}_n(t; \boldsymbol{\mu}) = W^T \mathbf{f}(V \mathbf{u}_n(t; \boldsymbol{\mu}), t; \boldsymbol{\mu}) \quad (t, \boldsymbol{\mu}) \in \mathcal{T} \times \mathcal{P}, \quad (3.6)$$

we obtain another reduced system, which is a Petrov-Galerkin method.

Suppose U_h is a Hilbert space spanned by all N_h -dimensional vectors with respect to the appropriate inner product. $S_h \subset U_h$ is low-dimensional solution manifold. We try to find a n -dimensional subspace S_n to approximate S_h , the degree of approximation is characterized by the Kolmogorov n -width

$$d_n(S_h; U_h) := \inf_{\substack{S_n \subset U_h \\ \dim(S_n)=n}} d(S_h; S_n) = \inf_{\substack{S_n \subset U_h \\ \dim(S_n)=n}} \sup_{\boldsymbol{\mu} \in \mathcal{P}} \inf_{\mathbf{u}_n \in S_n} \|\mathbf{u}_h(\boldsymbol{\mu}) - \mathbf{u}_n\|_{U_h},$$

where $d(S_h; S_n)$ is the maximum distance between S_n and S_h . Theories show that Kolmogorov n -width decreases with the increase of n , but the decay rate depends on the problem [29]. For the linear trial subspace S_n generated by POD, the Kolmogorov n -width defined above decays quickly for diffusion-dominant problems. However, Kolmogorov n -width decays slowly for convection-dominant problems. We must increase the order of ROM largely to obtain the required accuracy [29]. Next, we introduce a convolutional autoencoder based nonlinear ROM.

3.2 Convolutional autoencoder based nonlinear ROM

Autoencoder is a kind of feedforward neural network that learns identical mapping, which consists of two parts: encoder \mathbf{h}_{enc} and decoder \mathbf{h}_{dec} . Encoder maps \mathbf{u}_h to a low-dimensional vector \mathbf{u}_n

$$\begin{aligned} \mathbf{h}_{\text{enc}} : \mathbb{R}^{N_h} &\rightarrow \mathbb{R}^n \\ \mathbf{u}_h &\mapsto \mathbf{u}_n, \end{aligned} \quad (3.7)$$

where $n \ll N_h$. Decoder maps \mathbf{u}_n to an approximation of FOM solution \mathbf{u}_h

$$\begin{aligned} \mathbf{h}_{\text{dec}} : \mathbb{R}^n &\rightarrow \mathbb{R}^{N_h} \\ \mathbf{u}_n &\mapsto \tilde{\mathbf{u}}_h. \end{aligned} \quad (3.8)$$

Therefore, autoencoder can be written in the following form

$$\mathbf{h} : \mathbf{u}_h \mapsto \mathbf{h}_{\text{dec}} \circ \mathbf{h}_{\text{enc}}(\mathbf{u}_h). \quad (3.9)$$

The encoder contains L layers network

$$\begin{cases} \mathbf{u}_n^{(0)} = \mathbf{u}_h \in \mathbb{R}^{N_h} \\ \mathbf{u}_n^{(l)} = \varphi(\mathbf{h}_{\text{enc}}^l(\mathbf{u}_n^{(l-1)})), \quad l = 1, \dots, L-1, \\ \mathbf{u}_n = \mathbf{u}_n^{(L)} = \mathbf{h}_{\text{enc}}^L(\mathbf{u}_n^{(L-1)}) \in \mathbb{R}^n, \end{cases} \quad (3.10)$$

where $\mathbf{u}_n^{(l)}$ represents the l -layer output. $\mathbf{h}_{\text{enc}}^l$ represents the l -layer network operator, such as convolution or fully connection. φ is a nonlinear activation function. The decoder contains L layers network

$$\begin{cases} \tilde{\mathbf{u}}_h^{(0)} = \mathbf{u}_n \in \mathbb{R}^n \\ \tilde{\mathbf{u}}_h^{(l)} = \varphi\left(\mathbf{h}_{\text{dec}}^l(\tilde{\mathbf{u}}_h^{(l-1)})\right), \quad l = 1, \dots, L-1, \\ \tilde{\mathbf{u}}_h = \tilde{\mathbf{u}}_h^{(L)} = \mathbf{h}_{\text{dec}}^L(\tilde{\mathbf{u}}_h^{(L-1)}) \in \mathbb{R}^{N_h}. \end{cases} \quad (3.11)$$

Different architecture in the autoencoder leads to different method. Fully connected layers have good expressivity, Refs [30, 31, 32] choose all layers as fully connected layers then get multilayer perceptron autoencoder (MLPAE), which is effective for small-scale systems. However, for large-scale systems, the required training parameters in MLPAE will increase dramatically, which results in a curse of dimension. For example, when N_h is about 10^6 , even if only one fully connected layer is used to reduce the high fidelity vector to 100-dimension, the network parameters will exceed 10^8 . Therefore, it requires to reduce parameters in MLPAE. An alternative is the convolutional autoencoder (CAE). CAE uses a parameter sharing mechanism to reduce the training parameters. It brings the benefit of reducing the data required for network training. In addition, convolutional networks also have the characteristics of local connectivity, and translation invariance etc.[33, 34]. However, when we try to choose all layers as convolutional layers, we find that this sometimes leads to an insufficient network expressivity. Therefore, consider the number of parameters and expressivity together, Refs [23, 35, 1] combine the fully connected layers and the convolutional layers.

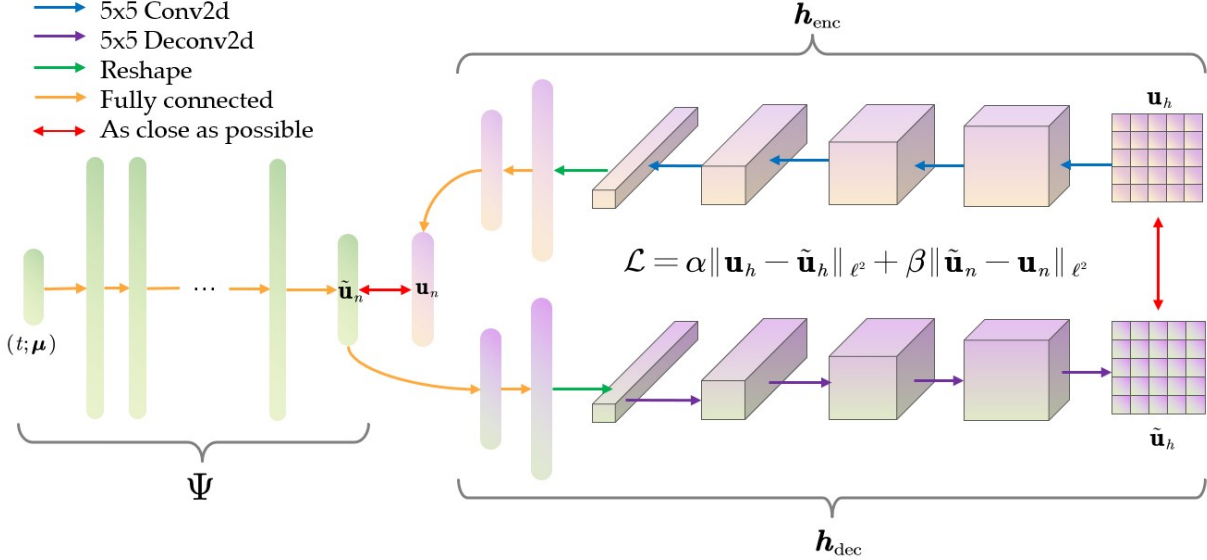


Figure 1: **DL-ROM**: The network architecture proposed in [1]. *Upper right*: \mathbf{h}_{enc} converts original data \mathbf{u}_h into a latent representation \mathbf{u}_n ; *Lower right*: \mathbf{h}_{dec} recovers data from low-dimensional solution $\tilde{\mathbf{u}}_n$; *Left*: Ψ is to fit the low-dimensional solution map.

Figure 1 shows a ROM based on CAE, called DL-ROM. \mathbf{h}_{enc} represents the encoder. It is a 6-layers network, where the first four layers are convolutional layers, and the last two layers are fully connected layers. θ_E represents the network parameters of \mathbf{h}_{enc} , then formula (3.10) can be written as

$$\mathbf{u}_n = \mathbf{h}_{\text{enc}}(\mathbf{u}_h; \theta_E). \quad (3.12)$$

Ψ is the low-dimensional solution map

$$\tilde{\mathbf{u}}_n = \Psi(t, \mu; \theta_F), \quad (3.13)$$

where θ_F represents the network parameters of Ψ . We expect its output $\tilde{\mathbf{u}}_n$ is as close to the encoder output \mathbf{u}_n as possible. DL-ROM uses $\Phi := \mathbf{h}_{\text{dec}} \circ \Psi$ to approximate the solution map

$$\tilde{\mathbf{u}}_h = \mathbf{h}_{\text{dec}}(\tilde{\mathbf{u}}_n; \theta_D), \quad (3.14)$$

where θ_D represents the network parameters of \mathbf{h}_{dec} . It is also a 6-layers network, where the first two layers are fully connected, the last four layers are deconvolutional layers.

The training of DL-ROM is carried out on its three subnets $\mathbf{h}_{\text{enc}}, \mathbf{h}_{\text{dec}}, \Psi$ simultaneously, hence the loss function includes both the autoencoder error and the low-dimensional fitting error

$$\min_{\boldsymbol{\theta}} \mathcal{J}(\boldsymbol{\theta}) = \min_{\boldsymbol{\theta}} \frac{1}{N_s} \sum_{i=1}^{N_{\text{train}}} \sum_{k=1}^{N_t} \mathcal{L}(t^k, \boldsymbol{\mu}_i; \boldsymbol{\theta}), \quad (3.15)$$

where

$$\mathcal{L}(t^k, \boldsymbol{\mu}_i; \boldsymbol{\theta}) = \alpha \|\mathbf{u}_h(t^k; \boldsymbol{\mu}_i) - \tilde{\mathbf{u}}_h(t^k; \boldsymbol{\mu}_i, \boldsymbol{\theta}_F, \boldsymbol{\theta}_D)\|_{\ell^2} + \beta \|\tilde{\mathbf{u}}_n(t^k; \boldsymbol{\mu}_i, \boldsymbol{\theta}_E) - \mathbf{u}_n(t^k; \boldsymbol{\mu}_i, \boldsymbol{\theta}_D)\|_{\ell^2}. \quad (3.16)$$

$\boldsymbol{\theta} = (\boldsymbol{\theta}_E, \boldsymbol{\theta}_D, \boldsymbol{\theta}_F)$, $\alpha, \beta \in (0, 1)$ are hyperparameters. Algorithm 1 and Algorithm 2 summarize the training and testing process of DL-ROM, respectively.

Algorithm 1: DL-ROM offline training

Data: Parameter matrix $P \in \mathbb{R}^{(n_\mu+1) \times N_s}$, snapshot matrix $S \in \mathbb{R}^{N_h \times N_s}$

Input: The number of training epochs N_{epochs} , batch size N_b , learning rate η , learning rate adjustment strategy, early stopping patiences, hyperparameter α, β

Output: Trained model $\mathbf{h}_{\text{enc}}, \mathbf{h}_{\text{dec}}, \Psi$

- 1 Data preprocess on S and scale it to $[0, 1]$
 - 2 Randomly shuffle P, S , and split them into training set $(P^{\text{train}}, S^{\text{train}})$ and validation set $(P^{\text{val}}, S^{\text{val}})$ according to the ratio of 8:2
 - 3 Generate data loader according to batch size N_b
 - 4 Define model $\mathbf{h}_{\text{enc}}, \mathbf{h}_{\text{dec}}, \Psi$ and initialize the model parameters through the Kaiming uniform initialization[36]
 - 5 **while** $n_{\text{epochs}} \leq N_{\text{epochs}}$ **do**
 - 6 **for** $(P^{\text{batch}}, S^{\text{batch}})$ in train-loader **do**
 - 7 Encode S^{batch} according to equation (3.12) to get $\widetilde{S}_n^{\text{batch}}$
 - 8 Compute equation (3.13) for all $t, \boldsymbol{\mu}$ in P^{batch} to get $\widetilde{S}_n^{\text{batch}}$
 - 9 Decode $\widetilde{S}_n^{\text{batch}}$ according to equation (3.14) to get $\widetilde{S}^{\text{batch}}$
 - 10 Computing loss function (3.15)
 - 11 Backpropagate
 - 12 Apply Adam algorithm to update model parameters
 - 13 **end**
 - 14 **for** $(P^{\text{batch}}, S^{\text{batch}})$ in val-loader **do**
 - 15 Do 7-10 similar to what was done on training set
 - 16 **if** early-stopping **then**
 - 17 **return** trained model $\mathbf{h}_{\text{enc}}, \mathbf{h}_{\text{dec}}, \Psi$
 - 18 **end**
 - 19 **end**
 - 20 Adjust the learning rate
 - 21 $n_{\text{epochs}} = n_{\text{epochs}} + 1$.
 - 22 **end**
 - 23 **return** trained model $\mathbf{h}_{\text{enc}}, \mathbf{h}_{\text{dec}}, \Psi$
-

Algorithm 2: DL-ROM online testing

Data: Testing parameter matrix $P \in \mathbb{R}^{(n_\mu+1) \times N_s}$

Input: Trained model $\Psi, \mathbf{h}_{\text{dec}}$ by Algorithm 1

Output: Predicted solution matrix \tilde{S} corresponding to the parameter matrix P

- 1 Compute equation (3.13) for all $t, \boldsymbol{\mu}$ in P to get \widetilde{S}_n
 - 2 Decode \widetilde{S}_n according to equation (3.14) to get \tilde{S} .
-

4 Observation

This section first repeats numerical experiments of the 1D viscous Burgers equation in [1]. Then we change the parameter range and use DL-ROM to solve it again. Numerical results show that DL-ROM cannot capture the drastic change of solution when the equation becomes diffusion-dominant. We give an explanation for this phenomenon.

Consider the following 1D viscous Burgers equation

$$\begin{cases} \frac{\partial u}{\partial t} + u \frac{\partial u}{\partial x} - \frac{1}{\mu} \frac{\partial^2 u}{\partial x^2} = 0, & (x, t) \in (0, L) \times (0, T) \\ u(0, t) = 0, & t \in (0, T) \\ u(L, t) = 0, & t \in (0, T) \\ u(x, 0) = u_0(x), & x \in (0, L) \end{cases} \quad (4.1)$$

where initial value

$$u_0(x) = \frac{x}{1 + \sqrt{1/A_0} \exp(\mu x^2/4)}, \quad (4.2)$$

and $A_0 = \exp(\mu/8)$, $L = 1$, $T = 2$, $\mu \in \mathcal{P} \subset \mathbb{R}^{n_\mu}$ is the single parameter ($n_\mu = 1$). The numerical methods used here are linear FEM with $N_h = 256$ grid points, and backward Euler with $N_t = 100$ time layers.

As Ref [1] does, the parameter range is $\mathcal{P} = [100, 1000]$, and the corresponding viscosity coefficient $1/\mu$ belongs to $[10^{-3}, 10^{-2}]$. This means that equation (4.1) is a convection-dominated equation. We randomly sample $N_{\text{train}} = 20$ parameters in the parameter range according to the uniform distribution. The midpoint of every two training parameters is used as test parameter, i.e., $N_{\text{test}} = 19$. After sampling, we solve the corresponding equation (4.1) by the above numerical methods, and assemble the parameters and corresponding high-fidelity solutions into a parameter matrix $P \in \mathbb{R}^{(n_\mu+1) \times N_s}$, and a snapshot matrix $S \in \mathbb{R}^{N_h \times N_s}$.

We use Pytorch[37] as a implementation platform for training the network and predicting results. The concrete network architecture is as follows. Ψ contains 10 hidden layers, and each layer contains 50 neurons. The nonlinear activation function used here is ELU [38]. Table 1 shows the parameters of \mathbf{h}_{enc} , \mathbf{h}_{dec} . Furthermore, we found that increasing the number of network layers will hardly affect the generalization ability of DL-ROM.

Table 1: Network architecture used in 1D viscous Burgers equation experiment. N_b represents batch size. Notations in Conv2d and ConvTranspose2d are: i: in channels; o: out channels; k: kernel size; s: stride; p: padding.

\mathbf{h}_{enc} (input shape: $(N_b, 256)$)		\mathbf{h}_{dec} (input shape: (N_b, n))	
Layer type	Output shape	Layer type	Output shape
Reshape	$(N_b, 1, 16, 16)$	Fully connected	$(N_b, 256)$
Conv2d(i=1, o=8, k=5, s=1, p=2)	$(N_b, 8, 16, 16)$	Fully connected	$(N_b, 256)$
Conv2d(i=8, o=16, k=5, s=2, p=2)	$(N_b, 16, 8, 8)$	Reshape	$(N_b, 64, 2, 2)$
Conv2d(i=16, o=32, k=5, s=2, p=2)	$(N_b, 32, 4, 4)$	ConvTranspose2d(i=64, o=64, k=5, s=3, p=2)	$(N_b, 64, 4, 4)$
Conv2d(i=32, o=64, k=5, s=2, p=2)	$(N_b, 64, 2, 2)$	ConvTranspose2d(i=64, o=32, k=5, s=3, p=1)	$(N_b, 32, 12, 12)$
Reshape	$(N_b, 256)$	ConvTranspose2d(i=32, o=16, k=5, s=1, p=1)	$(N_b, 16, 14, 14)$
Fully connected	$(N_b, 256)$	ConvTranspose2d(i=16, o=1, k=5, s=1, p=1)	$(N_b, 1, 16, 16)$
Fully connected	(N_b, n)	Reshape	$(N_b, 256)$

We use Adam algorithm [39] to train the network, the initial learning rate is set to $\eta = 10^{-4}$, the batch size is $N_b = 20$. We set early stopping patiences to 500. In other words, we stop training if error on the validation set does not decrease for 500 consecutive epochs. Under these settings, we apply Algorithm 1 for training. In the case of a fixed time-parameter instance, define its relative error as

$$\mathcal{E}_{\text{single}} = \frac{\|\mathbf{u}_h(\boldsymbol{\mu}, t) - \tilde{\mathbf{u}}_h(\boldsymbol{\mu}, t)\|_{\ell^2}}{\|\mathbf{u}_h(\boldsymbol{\mu}, t)\|_{\ell^2}}. \quad (4.3)$$

The average relative error in the entire test set is defined as

$$\mathcal{E}_{\text{total}} = \frac{1}{N_{\text{test}}} \sum_{i=1}^{N_{\text{test}}} \left(\frac{\sum_{k=1}^{N_t} \|\mathbf{u}_h^k(\boldsymbol{\mu}_{\text{test}}, i) - \tilde{\mathbf{u}}_h^k(\boldsymbol{\mu}_{\text{test}}, i)\|_{\ell^2}}{\sum_{k=1}^{N_t} \|\mathbf{u}_h^k(\boldsymbol{\mu}_{\text{test}}, i)\|_{\ell^2}} \right). \quad (4.4)$$

Figure 2 compares the results of using POD and DL-ROM to solve the equation (4.1) corresponding to parameter $\mu_{\text{test}} = 893.53$ at $t = 0.02$, using the FOM solution as a reference. We can observe that when solving this parameter with the same reduced dimension, DL-ROM has higher accuracy.

Figure 3 displays the change of the average relative error of the test set (4.4). We can find that when n is smaller, the approximation of DL-ROM is better than POD. These results are consistent with paper[1].

Next we change the parameter range to $\mathcal{P} = [0.5, 2]$, and its corresponding viscosity coefficient $1/\mu$ belongs to $[0.5, 2]$. We also sample $N_{\text{train}} = 20$ parameters in \mathcal{P} according to the uniform distribution to generate the training set

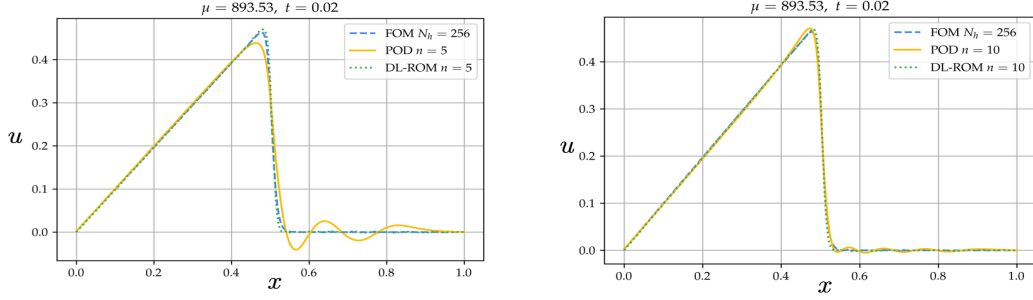


Figure 2: FOM, POD and DL-ROM solutions of parameter $\mu_{\text{test}} = 893.53$ at $t = 0.02$. The dimension of the reduced space: left $n = 5$, right $n = 10$.

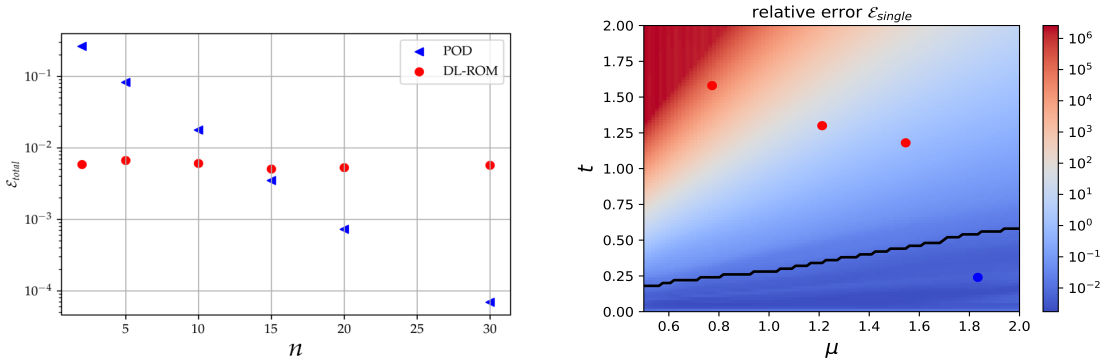


Figure 3: The average relative error of POD and DL-ROM on the test set, where $\mathcal{E}_{\text{total}}$ is defined in (4.4). Figure 4: The relative error of DL-ROM solving viscous Burgers equation on the test set.

($N_h = 256, N_t = 100$). The test set is obtained by sampling $N_{\text{test}} = 100$ parameters equidistantly in the parameter range.

Figure 4 shows the relative error of the DL-ROM's prediction results for each parameter in the test set. The relative error above the black line is greater than 10^{-2} , and below is less than 10^{-2} . Figure 5 shows DL-ROM's inference results of the parameters corresponding to the four marked points in Figure 4. This implies that DL-ROM's generalization ability becomes weakened.

The reason is attributed to the fact that when the parameter range is set to $\mathcal{P} = [0.5, 2]$, the diffusion term in the equation (4.1) plays a role, causing its solution to change drastically along the time direction. We define the following γ to quantify the severity of the solution change

$$\gamma = \frac{\max_{\mu \in \mathcal{P}} \|\mathbf{u}_h(\cdot, \mu)\|_{\ell^\infty}}{\min_{\mu \in \mathcal{P}} \|\mathbf{u}_h(\cdot, \mu)\|_{\ell^\infty}}. \quad (4.5)$$

The larger the γ , the more drastic the solution changes, and vice versa. For viscous Burgers equation (4.1), when $\mathcal{P} = [100, 1000]$, $\log_{10} \gamma < 2$, the solution does not change much and DL-ROM has good generalization ability. On the contrary, when $\mathcal{P} = [0.5, 2]$, $\log_{10} \gamma > 2$, the solution changes drastically, DL-ROM is inclined to fit the solution whose norm is relatively large but ignore solutions with relatively small norms. This observation inspires us to classify the original dataset and establish a classification network based on the classified data.

5 Multiclass classification-based ROM

Inspired by the observation above, in this section, we design the MC-ROM and analyze its computational complexity of online computation.

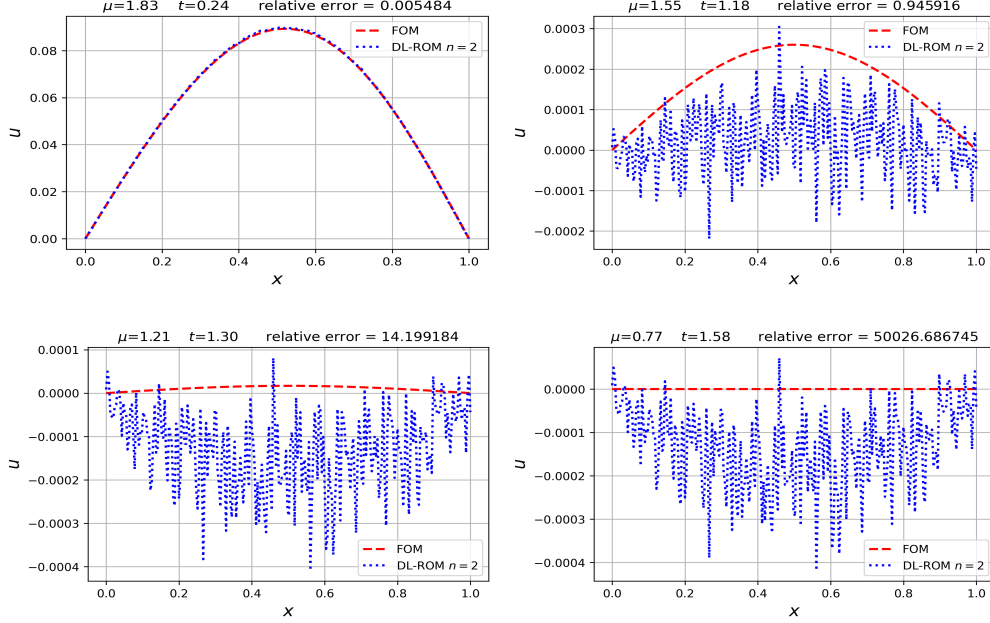


Figure 5: The results of viscous Burgers equation corresponding to the marked parameters in Figure 4.

5.1 Network architecture

Figure 6 gives the network architecture of MC-ROM. The blue block on the left plot is the classifier, and its purpose is to classify the parameters according to the order of magnitude of the numerical solution. Its input is (t, μ) , and the output is the label to classify the data. In practice, we use the order of magnitude of ℓ^∞ norm of numerical solution as classification criteria to assign each parameter a label. We then use parameter-label pairs as the training dataset for the classifier.

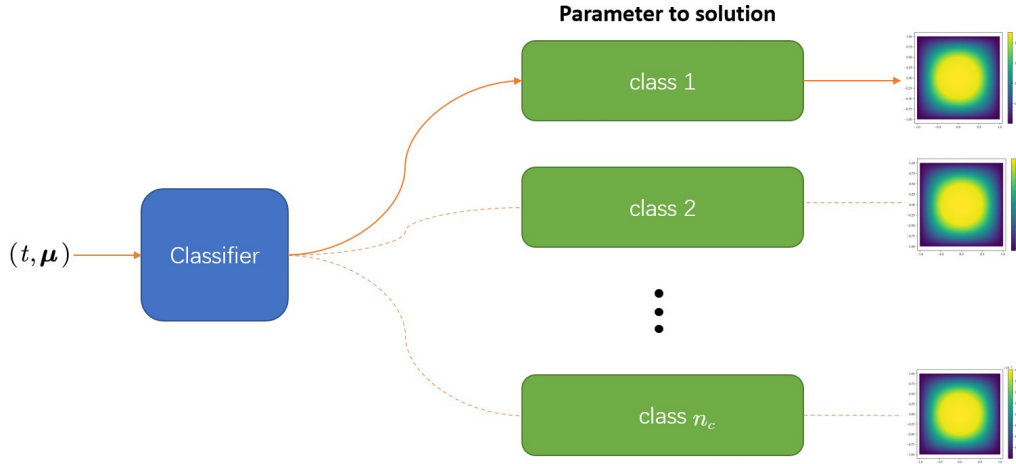


Figure 6: MC-ROM network architecture.

There are many classification algorithms, such as neural networks, decision trees, k-nearest neighbors, naive Bayes, etc. The choice of classification depends on the problem. Here, we choose SVM to train the classifier due to the small training data. For our numerical results, SVM has better performance than fully connected neural networks. As shown in Figure 7, SVM separates different types of data by constructing a hyperplane or a group of hyperplanes in

a high-dimensional or infinite-dimensional space. The distance between different classes is called margin. Generally, the larger the margin, the smaller the generalization error of the classifier, so the hyperplane should be constructed so that the distance from the nearest training data point of any class is large enough. SVM applies the kernel trick to make the data set linearly separable and uses Higen loss to achieve these hyperplanes to meet the above properties. See Refs [40, 41] for a detailed description. We implement SVM through sklearn [42].

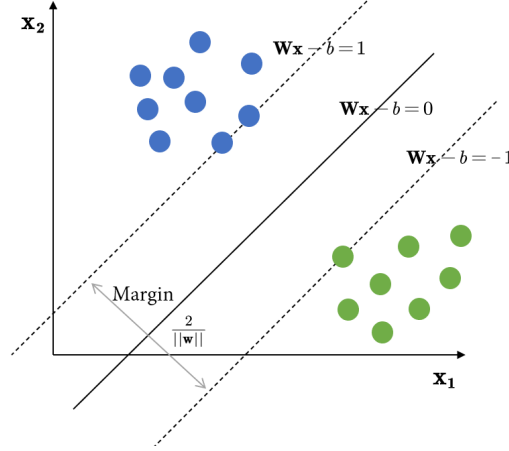


Figure 7: SVM is to maximum the margin.

The green blocks on the right plot are different subnets. Each subnet is used to fit the parameter to solution mapping in a certain class. The subnet architectures can be the same or different, depending on the problem. Here, all of our subnet models are DL-ROM due to its high efficiency of online computing and its applicability to convection problems. The offline training process of different subnets are similar learning tasks, and we can apply transfer learning [43] to speed up training. In transfer learning, when the training of a subnet is completed, its parameters can assign to the next subnet as the initial parameters for training. The numerical experiment in Section 6.1 will show the advantages of transfer learning. The offline training and online testing of MC-ROM are summarized in Algorithm 3 and Algorithm 4.

Algorithm 3: MC-ROM offline training

Data: Parameter matrix $P \in \mathbb{R}^{(n_\mu+1) \times N_s}$, snapshot matrix $S \in \mathbb{R}^{N_h \times N_s}$

Input: The number of training epochs N_{epochs} , batch size N_b , learning rate η , hyperparameter α, β

Output: A classifier \mathcal{C} and trained models $\mathbf{h}_{\text{enc}}^i, \mathbf{h}_{\text{dec}}^i, \Psi^i, i = 1, \dots, n_c$

- 1 Classify P and S into $[P_1, \dots, P_{n_c}]$ and $[S_1, \dots, S_{n_c}]$ and get label matrix $L \in \mathbb{R}^{n_c \times N_s}$
 - 2 Use SVM to train a classifier \mathcal{C} with P and L
 - 3 **for** $i = 1 : n_c$ **do**
 - 4 Substitute the data P_i, S_i into Algorithm 1 and use DL-ROM input parameters to train to get $\mathbf{h}_{\text{enc}}^i, \mathbf{h}_{\text{dec}}^i, \Psi^i$
 - 5 **end**
 - 6 **return** \mathcal{C} and $\mathbf{h}_{\text{enc}}^i, \mathbf{h}_{\text{dec}}^i, \Psi^i, i = 1, \dots, n_c$
-

Algorithm 4: MC-ROM online testing

Data: Parameter matrix $P \in \mathbb{R}^{(n_\mu+1) \times N_s}$

Input: Algorithm 3 trained model \mathcal{C} and $\Psi^i, \mathbf{h}_{\text{dec}}^i; i = 1, \dots, n_c$

Output: The predicted solution matrix \tilde{S} corresponding to the parameter matrix P

- 1 Substitutethe parameters into the classifier \mathcal{C} to determine which class it belongs to
 - 2 Substitute the parameters into the corresponding trained model $\mathbf{h}_{\text{dec}}^i \circ \Psi^i$ to get \tilde{S}
-

5.2 Computational complexity

This subsection analyzes the online computational complexity of MC-ROM and POD. We make a convention that

$$\mathbb{A}_h(\boldsymbol{\mu})\mathbf{u}_h(\boldsymbol{\mu}) = \mathbf{f}_h(\boldsymbol{\mu}), \quad (5.1)$$

represents the FOM system, where $\mathbb{A}_h(\boldsymbol{\mu}) \in \mathbb{R}^{N_h \times N_h}$, and

$$\mathbb{A}_n(\boldsymbol{\mu})\mathbf{u}_n(\boldsymbol{\mu}) = \mathbf{f}_n(\boldsymbol{\mu}), \quad (5.2)$$

represents the reduced system, $\mathbb{A}_n(\boldsymbol{\mu}) \in \mathbb{R}^{n \times n}$, n may be much smaller than N_h .

The online calculation of MC-ROM has two steps except classification:

1. Solve \mathbf{u}_n . Use a fully connected network to approximate $\mathbf{u}_n(\boldsymbol{\mu})$, the computational amount of each layer is N_{neu}^2 . If there are l hidden layers, the computational amount is $l \times N_{\text{neu}}^2$ except the input and output layers;
2. Lift \mathbf{u}_n to high-dimensional manifold through the decoder. The computational amount of a deconvolution layer is $O(N_h \cdot k^2 \cdot C_{\text{in}} \cdot C_{\text{out}})$, where k^2 is the size of the convolution kernel. C_{in} and C_{out} represent the number of channels of the previous layer and the current layer.

In actual calculations, N_{neu} , l , k , C_{in} , C_{out} are much smaller than N_h , then the online computational complexity of MC-ROM is $O(N_h)$.

The online stage of POD can has the following four steps:

1. Given a $\boldsymbol{\mu}$, discrete its corresponding PDE to get (5.1);
2. Project the linear system (5.1) to a low-dimensional manifold and get (5.2), where

$$\mathbb{A}_n = V^T \mathbb{A}_h V, \quad \mathbf{f}_n = V^T \mathbf{f}_h. \quad (5.3)$$

and $V \in \mathbb{R}^{N_h \times n}$ is obtained in POD offline stage;

3. Solve (5.2);
4. Lift the low-dimensional solution $\mathbf{u}_n(\boldsymbol{\mu})$ to high-dimensional manifold $V\mathbf{u}_n(\boldsymbol{\mu})$.

The computational complexity corresponding to each step above is as follows:

1. Use spatial discretization methods such as FEM, FDM to obtain (5.1), computational complexity depends on the discretization methods used;
2. Projecte it to a low-dimensional manifold requires matrix multiplication, hence the computational complexity is $O(N_h^2)$;
3. Equation (5.2) is dense, the computational complexity of directly solving it is $O(n^3)$;
4. Lift operation is $V\mathbf{u}_n(\boldsymbol{\mu})$, the operations required is $N_h \times n$.

Sometimes, the first two parts can be put offline. For example, if $\mathbb{A}_h(\boldsymbol{\mu})$ and $\mathbf{f}_h(\boldsymbol{\mu})$ in (5.1) are **parameter-separable**, i.e.

$$\mathbb{A}_h(\boldsymbol{\mu}) = \sum_{q=1}^{Q_a} \theta_a^q(\boldsymbol{\mu}) \mathbb{A}_h^q, \quad \mathbf{f}_h(\boldsymbol{\mu}) = \sum_{q=1}^{Q_f} \theta_f^q(\boldsymbol{\mu}) \mathbf{f}_h^q, \quad (5.4)$$

where $\theta_a^q : \mathcal{P} \rightarrow \mathbb{R}$, $q = 1, \dots, Q_a$ and $\theta_f^q : \mathcal{P} \rightarrow \mathbb{R}$, $q = 1, \dots, Q_f$. Then we can apply Galerkin method (3.5) to (5.4) and get

$$\mathbb{A}_n(\boldsymbol{\mu}) = \sum_{q=1}^{Q_a} \theta_a^q(\boldsymbol{\mu}) \mathbb{A}_n^q, \quad \mathbf{f}_n(\boldsymbol{\mu}) = \sum_{q=1}^{Q_f} \theta_f^q(\boldsymbol{\mu}) \mathbf{f}_n^q, \quad (5.5)$$

where $\mathbb{A}_n^q = V^T \mathbb{A}_h^q V$, $\mathbf{f}_n^q = V^T \mathbf{f}_h^q$ can be pre-calculated. In this case, the first two steps of POD online calculation are replaced by directly assembling equation (5.5). The operations required to generate (5.5) is $O(Q_a n^2 + Q_f n)$. If n and Q_a , Q_f are small enough, then the online computational complexity of POD is $O(N_h)$.

However, even for the parameter-separable problems, MC-ROM still has the following advantages over POD. Firstly, we noticed that the computational complexity of the third step of POD is $O(n^3)$. Therefore, when the problem to be solved requires a high-dimensional reduced space, the online calculation of POD will become costly. Secondly, using neural networks as the surrogate model to establish the mapping between parameters and solutions has fundamentally changed the calculation process of many scenarios in scientific computing. Compared with POD, MC-ROM is a non-intrusive ROM. The calculation based on the neural network makes it easier to use computing resources such as GPU, making its online calculation much faster than POD. Section 6 shows the related numerical experiments.

6 Numerical Experiments

This section applies MC-ROM to solve the 1D viscous Burgers equation and 2D parabolic equation with discontinuous diffusion coefficients. We also compare the approximation accuracy and computational time of solving these equations with DL-ROM and with POD. All the experiments in this section are done on a workstation equipped with two Intel(R) Xeon(R) Silver 4214 CPU @ 2.20GHz, 128GB RAM, and Nvidia Tesla V100-PCIe-32GB GPU.

6.1 1D viscous Burgers equation

In Section 4, we have used DL-ROM to solve the viscous Burgers equation (4.1) with parameter interval $\mathcal{P} = [0.5, 2]$, but its generalization ability is very poor. Here, we use MC-ROM to solve it. Firstly, we classify the original training dataset according to the FOM solution vectors. Concretely, we use two consecutive orders of magnitude of ℓ^∞ norm to label the parameters. We divide the original dataset into n_c classes, and the labels corresponding to all parameters are assembled into a label matrix $L \in \mathbb{R}^{n_c \times N_s}$. Table 2 shows the classification results of the training set.

Table 2: Classification results of the training set whose data are FOM solutions of 1D viscous Burgers equation.

Range of $\ \mathbf{u}_h\ _{\ell^\infty}$	$\ \mathbf{u}_h\ _{\ell^\infty} \geq 10^{-2}$	$[10^{-4}, 10^{-2})$	$[10^{-6}, 10^{-4})$	$[10^{-8}, 10^{-6})$	$[10^{-10}, 10^{-8})$	$\ \mathbf{u}_h\ _{\ell^\infty} \leq 10^{-10}$
Label	1	2	3	4	5	6
Size	435	573	477	224	244	67

Next we apply the dataset $\{p_i, l_i\}_{i=1}^{N_s}$ to train the SVM classifier, where p_i, l_i are the i -th column of parameter matrix $P \in \mathbb{R}^{(n_\mu+1) \times N_s}$ and label matrix $L \in \mathbb{R}^{n_c \times N_s}$, respectively. After training, we verify the performance of the classifier on the test set, and the result is that it has an accuracy of 97.17%, as shown in Figure 8. And we can see that the black line in the Figure 4 is very similar to the line between the first and second class in the Figure 8. These results demonstrate DL-ROM only approximates well for the first data class. In order to improve DL-ROM so that it has generalization ability for the entire parameter space, it is necessary to train with different subnets according to the classification result shown in Figure 8.

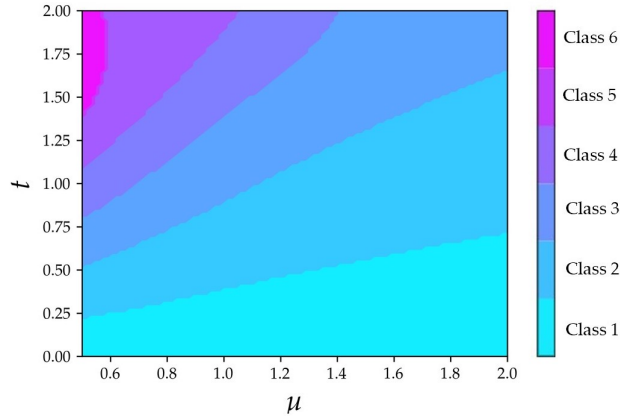


Figure 8: The classification result of the SVM classifier.

Finally, we apply Algorithm 1 to train each subnet. As mentioned in Section 5, we use transfer learning techniques to accelerate the offline training process. Figure 9 compares the impact of using transfer learning and randomly initialized network parameters during offline training. It can be seen that the former is more efficient.

Figure 10 compares the test results of MC-ROM, DL-ROM, and POD. The numerical results of DL-ROM in the last two plots are not shown since its relative error is too large. Compared to DL-ROM and POD, MC-ROM has good generalization ability for the parameters corresponding to solutions with different orders of magnitude.

Figure 11 shows the online computational time of POD and MC-ROM in solving 100 PPDEs in the test set. We can see that MC-ROM is much faster than POD, and it is not influenced by the dimension of the reduced space. This result is consistent with the computational complexity analysis in the Section 5.2.

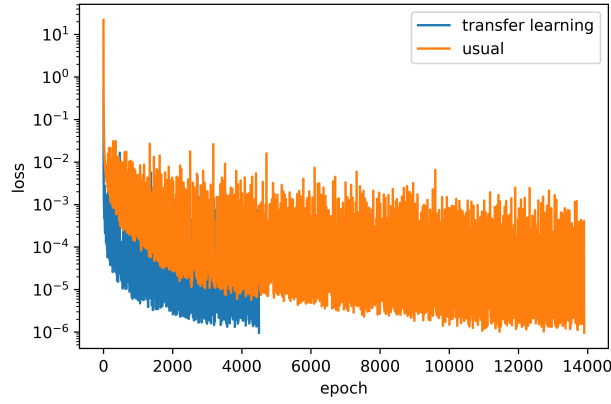


Figure 9: Comparison of the training process with and without transfer learning.

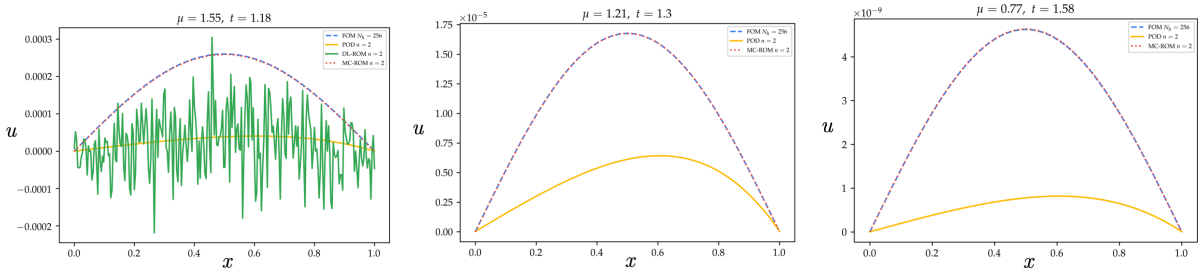
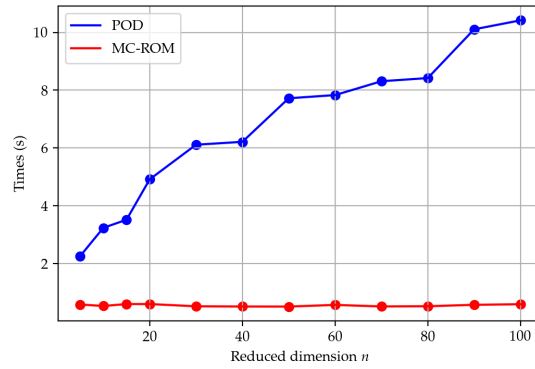

 Figure 10: Results of Solving equation (4.1) corresponding to the red marked parameters in Figure 4 by using POD, DL-ROM, and MC-ROM. n represents the dimension of the reduced space.


Figure 11: Comparison of online calculation time between POD and MC-ROM.

6.2 2D parabolic equation

Consider the following parabolic equation with discontinuous diffusion coefficient

$$\begin{cases} \partial_t u(t; \boldsymbol{\mu}) - \operatorname{div}(\kappa(\mu_0) \nabla u(t; \boldsymbol{\mu})) = 0 & \text{in } \Omega \times [0, T], \\ u(t=0; \boldsymbol{\mu}) = \mu_1(x-1)(x+1)(y-1)(y+1) & \text{in } \Omega, \\ u = 0 & \text{on } \partial\Omega, \end{cases} \quad (6.1)$$

where $T = 3$, $\Omega = (-1, 1)^2$ is divided into Ω_1 and Ω_2

- Ω_1 is a disk centered at the origin of radius $r_0 = 0.5$, and
- $\Omega_2 = \Omega \setminus \overline{\Omega_1}$.

This equation contains two parameters μ_0 and μ_1 . μ_0 is related to the coefficient in Ω_1 , and μ_1 appears in the initial value. As shown in Figure 12, the coefficient κ is constant on Ω_1 and Ω_2 , i.e.

$$\kappa|_{\Omega_1} = \mu_0 \quad \text{and} \quad \kappa|_{\Omega_2} = 1. \quad (6.2)$$

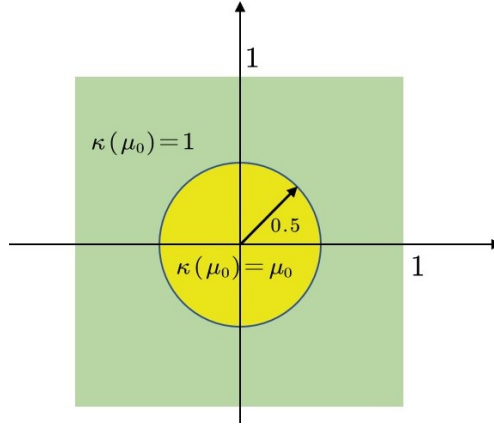


Figure 12: Distribution of coefficient κ .

We consider parameter $\boldsymbol{\mu} = (\mu_0, \mu_1) \in \mathcal{P} = [1, 10] \times [0.1, 10]$. As Figure 13 shows, we use Latin Hypercube Sampling [44] with a uniform distribution to generate a total of 300 parameters. According to the experience of the

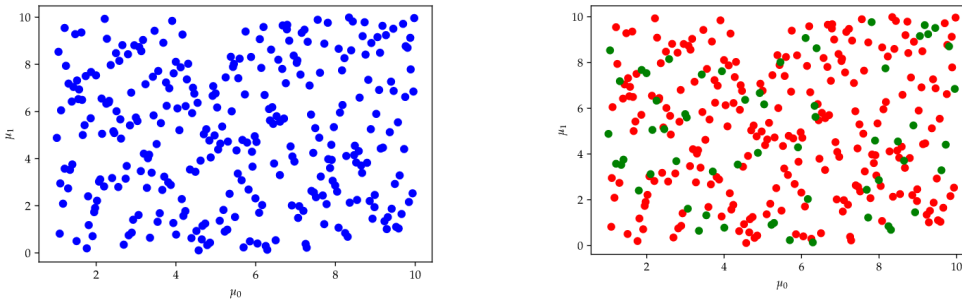


Figure 13: Left: Latin Hypercube Sampling with uniform distribution; Right: split left samples into training (red) and testing (green) samples.

training process of the viscous Burgers equation, the MC-ROM is not overfitting. Therefore, we divide the dataset into a training set and test set with the ratio of 8:2, i.e., 240 for training and 60 for testing, no longer leave for the validation set. Then we solve the corresponding high-fidelity solution for training and testing. For a given parameter, we use FEM and backward Euler methods to discretize space and time variable, respectively. And we use the software

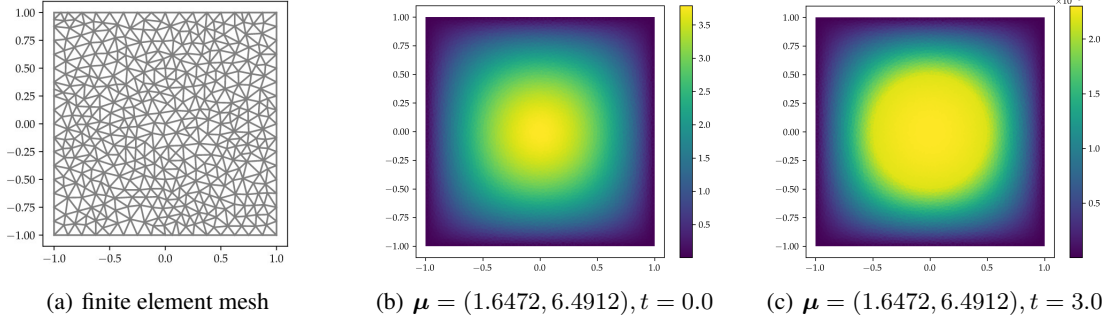


Figure 14: (a): Schematic diagram of mesh; (b,c): Numerical solution of equation (6.1) corresponding to $\mu = (1.6472, 6.4912)$ at initial and final time.

FEniCS[45] to implement the above numerical methods and obtain the dataset. Figure 14(a) shows a schematic mesh of spatial discretization. In practice, the mesh we use contains 5716 nodes and 11171 cells and $\Delta t = 0.5$. Figure 14(b) and Figure 14(c) show the FOM solution of parameter $(1.6472, 6.4912)$ at the initial and end moments. We can see that the order of magnitude of the solution is decreasing over time. Similar to the viscous Burgers equation, we classify training data using SVM. Table 3 presents the classification results.

Table 3: Classification results of the training set whose data are FOM solutions of the 2D parabolic equation.

Range of $\ \mathbf{u}_h\ _{\ell^\infty}$	$\ \mathbf{u}_h\ _{\ell^\infty} \geq 10^{-1}$	$[10^{-2}, 10^{-1})$	$[10^{-3}, 10^{-2})$	$[10^{-4}, 10^{-3})$	$[10^{-5}, 10^{-4})$	$\ \mathbf{u}_h\ _{\ell^\infty} \leq 10^{-5}$
Label	1	2	3	4	5	6
Size	3751	2346	2368	2360	2360	1455

The MC-ROM's subnets are all DL-ROM as shown in Figure 1, its concrete structure is as follows. Ψ contains 10 hidden layers, each layer contains 50 neurons. Table 4 shows the parameters of \mathbf{h}_{enc} , \mathbf{h}_{dec} . We use the Adam

Table 4: Network parameters of 2D Parabolic equation experiment. The meaning of parameters in Conv2d and ConvTranspose2d are: in channels(i), out channels(o), kernel size(k), stride(s), padding(p).

\mathbf{h}_{enc} (input shape: $(N_b, 5176)$)		\mathbf{h}_{dec} (input shape: (N_b, n))	
Layer type	Output shape	Layer type	Output shape
Fully connected	$(N_b, 4096)$	Fully connected	$(N_b, 256)$
Reshape	$(N_b, 1, 64, 64)$	Fully connected	$(N_b, 4096)$
Conv2d(i=1, o=8, k=5, s=1, p=2)	$(N_b, 8, 64, 64)$	Reshape	$(N_b, 64, 8, 8)$
Conv2d(i=8, o=16, k=5, s=2, p=2)	$(N_b, 16, 32, 32)$	ConvTranspose2d(i=64, o=64, k=5, s=3, p=2)	$(N_b, 64, 22, 22)$
Conv2d(i=16, o=32, k=5, s=2, p=2)	$(N_b, 32, 16, 16)$	ConvTranspose2d(i=64, o=32, k=5, s=3, p=2)	$(N_b, 32, 64, 64)$
Conv2d(i=32, o=64, k=5, s=2, p=2)	$(N_b, 64, 8, 8)$	ConvTranspose2d(i=32, o=16, k=5, s=1, p=2)	$(N_b, 16, 64, 64)$
Reshape	$(N_b, 4096)$	ConvTranspose2d(i=16, o=1, k=5, s=1, p=2)	$(N_b, 1, 64, 64)$
Fully connected	$(N_b, 256)$	Reshape	$(N_b, 4096)$
Fully connected	(N_b, n)	Fully connected	$(N_b, 5176)$

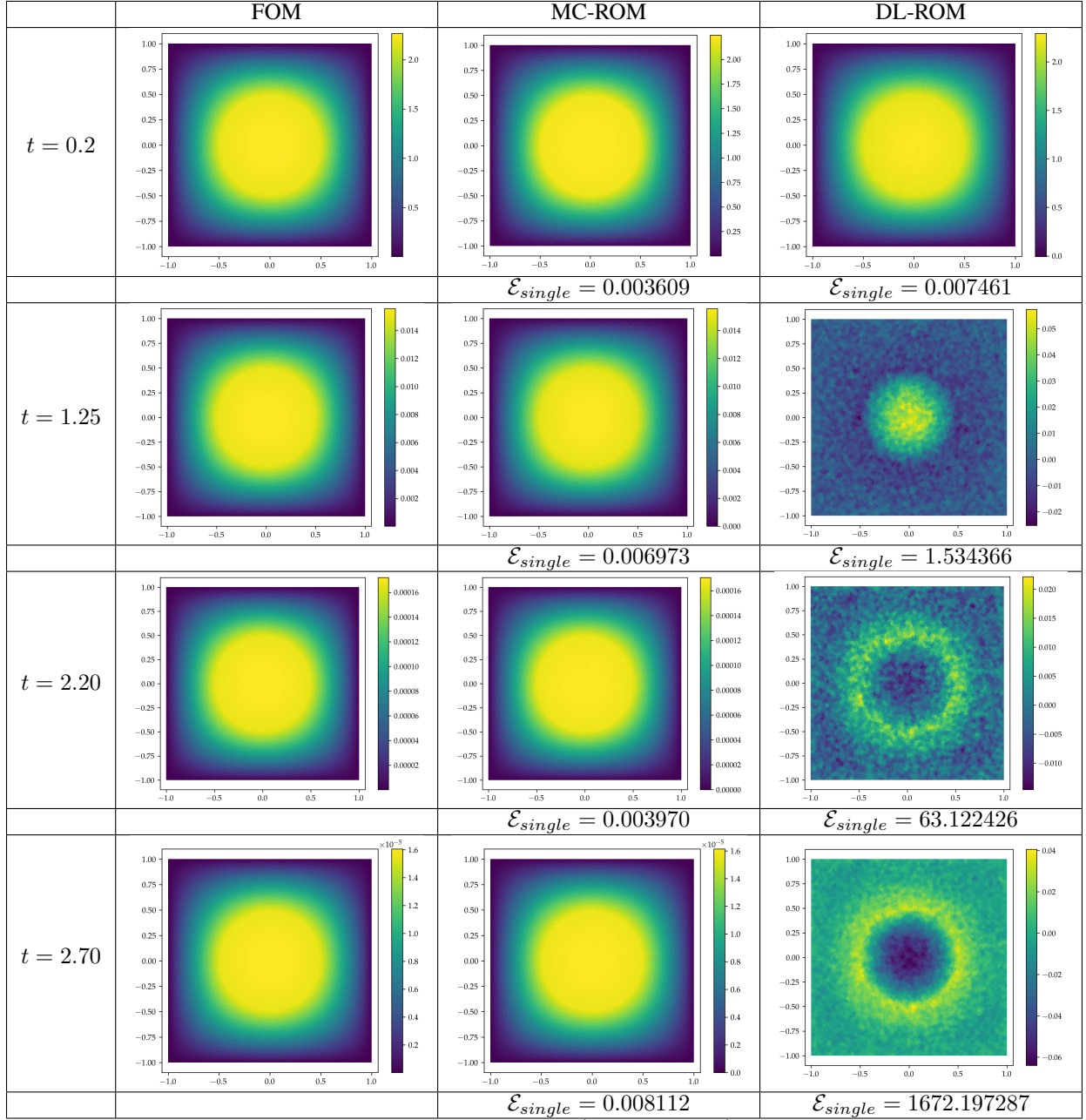
algorithm, and the initial learning rate is set to $\eta = 0.001$. A multi-step decay learning rate adjustment strategy is used, i.e., the current learning rate is reduced by 0.1 when epochs become 5000 and 10000. The maximum training epoch is $N_{\text{epochs}} = 20000$, and the batch size is $N_b = 5000$. We take $n = 5$ and apply Algorithm 3 to train MC-ROM.

Figure 6 shows the solutions of PDE (6.1) at time $t = 0.2, 1.25, 2.20, 2.70$ when $\mu = (9.9560, 6.8453)$, obtained by FOM, MC-ROM, and DL-ROM, respectively. It also gives the relative error of MC-ROM and DL-ROM according to equation (4.3). We find that MC-ROM maintains a good approximation at different times. At the same time, DL-ROM becomes worse over time, which means that MC-ROM has a better generalization ability than DL-ROM. Similar results can be found for other parameters μ in the test set.

We also use POD with $n = 5$ to solve this problem. Table 5 shows the results of using POD and MC-ROM to solve some parameters in the test set. We can see that under the same dimension of the reduced space, the approximation of MC-ROM is slightly better than that of POD, and the calculation efficiency is about one hundred times faster than

Table 5: Comparison of the average relative error at each time layer and the online calculation time of MC-ROM and POD when solving PDE (6.1) with five parameters in the test set.

Parameter		$\mu = (1.2104, 3.5723)$	$\mu = (7.8971, 4.5858)$	$\mu = (3.4226, 7.4731)$	$\mu = (9.6112, 3.2874)$	$\mu = (6.1625, 2.0293)$
Relative error	MC-ROM	0.01094	0.00952	0.00781	0.00952	0.00940
	POD	0.05671	0.01363	0.01377	0.01409	0.01315
Time(s)	MC-ROM	0.00168	0.00282	0.00271	0.00210	0.00170
	POD	0.12193	0.38497	0.20498	0.21644	0.16388


 Table 6: Numerical results of solving PDE(6.1) when $\mu = (9.9560, 6.8453)$ by the FOM, the MC-ROM, and the DL-ROM at different times. The relative error \mathcal{E}_{single} is defined in (4.3).

POD. We also get similar results for other parameters in the test set. These results confirm that the proposed model is much more effective than POD.

7 Conclusion and discussions

This paper proposes the MC-ROM for solving time-dependent PPDEs. MC-ROM classifies the data according to the magnitude of the FOM solutions, constructs corresponding subnets for different data classes, and builds a classifier to integrate all subnets. In the offline stage, MC-ROM can use transfer learning techniques to accelerate the training of subnets with the same architecture. Numerical experiments show that MC-ROM has good generalization ability for both diffusion-dominant and convection-dominant problems. Compared with DL-ROM, MC-ROM maintains its advantages, including its good approximation and generalization ability for convection-dominant problems, efficient online calculation. More importantly, MC-ROM improves the generalization ability of DL-ROM for diffusion-dominant problems. And MC-ROM is much more efficient than POD when doing online computing. Even more, POD is not suitable for convection-dominant problems due to its poor approximation, while MC-ROM can maintain sufficient accuracy. In this work, we use the DL-ROM as subset due to its good approximation ability and efficient online calculation. In fact, the MC-ROM is a flexibly extended model. Any appropriate network that approximates the parameter-to-solution mapping can be used as a subnet in the MC-ROM.

There are still many works to be explored. For instance, the characteristic of PPDEs that this paper focuses on is that the magnitude of their solutions changes drastically along the time direction. Therefore, we regard time as a parameter that can solve this kind of PPDEs. However, there are many PPDEs whose solutions change drastically in space or in time-space, such as interface problems and multi-scale problems. In that case, we need to regard spatial coordinates as parameters. In addition, to train the network to achieve satisfactory approximation accuracy, the amount of required data increases exponentially with the rise of the parameter space's dimension, which will lead to the curse of dimension. Furthermore, we try to apply MC-ROM to more scientific and engineering problems.

References

- [1] Stefania Fresca, Luca Dede, and Andrea Manzoni. A comprehensive deep learning-based approach to reduced order modeling of nonlinear time-dependent parametrized pdes. *Journal of Scientific Computing*, 87(2):1–36, 2021.
- [2] Kyle Gallivan, Antoine Vandendorpe, and Paul Van Dooren. Model reduction via tangential interpolation. In *MTNS 2002 (15th Symp. on the Mathematical Theory of Networks and Systems)*, page 6, 2002.
- [3] Jan S Hesthaven, Benjamin Stamm, and Shun Zhang. Efficient greedy algorithms for high-dimensional parameter spaces with applications to empirical interpolation and reduced basis methods. *ESAIM: Mathematical Modelling and Numerical Analysis*, 48(1):259–283, 2014.
- [4] YC Liang, HP Lee, SP Lim, WZ Lin, KH Lee, and CG Wu. Proper orthogonal decomposition and its applications—part i: Theory. *Journal of Sound and vibration*, 252(3):527–544, 2002.
- [5] Gal Berkooz, Philip Holmes, and John L Lumley. The proper orthogonal decomposition in the analysis of turbulent flows. *Annual review of fluid mechanics*, 25(1):539–575, 1993.
- [6] Gitta Kutyniok, Philipp Petersen, Mones Raslan, and Reinhold Schneider. A theoretical analysis of deep neural networks and parametric pdes. *arXiv preprint arXiv:1904.00377*, 2019.
- [7] Jan S Hesthaven and Stefano Ubbiali. Non-intrusive reduced order modeling of nonlinear problems using neural networks. *Journal of Computational Physics*, 363:55–78, 2018.
- [8] Isaac E Lagaris, Aristidis Likas, and Dimitrios I Fotiadis. Artificial neural networks for solving ordinary and partial differential equations. *IEEE transactions on neural networks*, 9(5):987–1000, 1998.
- [9] George Cybenko. Approximation by superpositions of a sigmoidal function. *Mathematics of control, signals and systems*, 2(4):303–314, 1989.
- [10] Maziar Raissi, Paris Perdikaris, and George E Karniadakis. Physics-informed neural networks: A deep learning framework for solving forward and inverse problems involving nonlinear partial differential equations. *Journal of Computational Physics*, 378:686–707, 2019.
- [11] E Weinan and Bing Yu. The deep ritz method: a deep learning-based numerical algorithm for solving variational problems. *Communications in Mathematics and Statistics*, 6(1):1–12, 2018.
- [12] Jiequn Han, Arnulf Jentzen, and E Weinan. Solving high-dimensional partial differential equations using deep learning. *Proceedings of the National Academy of Sciences*, 115(34):8505–8510, 2018.

- [13] Qian Wang, Jan S Hesthaven, and Deep Ray. Non-intrusive reduced order modeling of unsteady flows using artificial neural networks with application to a combustion problem. *Journal of computational physics*, 384:289–307, 2019.
- [14] Toby Phillips, Claire E Heaney, Paul N Smith, and Christopher C Pain. An autoencoder-based reduced-order model for eigenvalue problems with application to neutron diffusion. *arXiv preprint arXiv:2008.10532*, 2020.
- [15] W Chen, Q Wang, JS Hesthaven, and C Zhang. Physics-informed machine learning for reduced-order modeling of nonlinear problems. *Preprint*, 2020.
- [16] Yin hao Zhu, Nicholas Zabaras, Phaedon-Stelios Koutsourelakis, and Paris Perdikaris. Physics-constrained deep learning for high-dimensional surrogate modeling and uncertainty quantification without labeled data. *Journal of Computational Physics*, 394:56–81, 2019.
- [17] Peter Benner, Serkan Gugercin, and Karen Willcox. A survey of projection-based model reduction methods for parametric dynamical systems. *SIAM review*, 57(4):483–531, 2015.
- [18] Lu Lu, Pengzhan Jin, and George Em Karniadakis. Deeponet: Learning nonlinear operators for identifying differential equations based on the universal approximation theorem of operators. *arXiv preprint arXiv:1910.03193*, 2019.
- [19] Sifan Wang, Hanwen Wang, and Paris Perdikaris. Learning the solution operator of parametric partial differential equations with physics-informed deeponets. *arXiv preprint arXiv:2103.10974*, 2021.
- [20] Zongyi Li, Nikola Kovachki, Kamyar Azizzadenesheli, Burigede Liu, Kaushik Bhattacharya, Andrew Stuart, and Anima Anandkumar. Fourier neural operator for parametric partial differential equations. *arXiv preprint arXiv:2010.08895*, 2020.
- [21] Kaushik Bhattacharya, Bamdad Hosseini, Nikola B Kovachki, and Andrew M Stuart. Model reduction and neural networks for parametric pdes. *arXiv preprint arXiv:2005.03180*, 2020.
- [22] Thomas O’Leary-Roseberry, Umberto Villa, Peng Chen, and Omar Ghattas. Derivative-informed projected neural networks for high-dimensional parametric maps governed by pdes. *arXiv preprint arXiv:2011.15110*, 2020.
- [23] Francisco J Gonzalez and Maciej Balajewicz. Deep convolutional recurrent autoencoders for learning low-dimensional feature dynamics of fluid systems. *arXiv preprint arXiv:1808.01346*, 2018.
- [24] Shady E Ahmed, Omer San, Adil Rasheed, and Traian Iliescu. A long short-term memory embedding for hybrid uplifted reduced order models. *Physica D: Nonlinear Phenomena*, page 132471, 2020.
- [25] Ricky TQ Chen, Yulia Rubanova, Jesse Bettencourt, and David K Duvenaud. Neural ordinary differential equations. In *Advances in neural information processing systems*, pages 6571–6583, 2018.
- [26] Julius Berner, Markus Dablander, and Philipp Grohs. Numerically solving parametric families of high-dimensional kolmogorov partial differential equations via deep learning. *Advances in Neural Information Processing Systems*, 33, 2020.
- [27] Alfio Quarteroni, Andrea Manzoni, and Federico Negri. *Reduced basis methods for partial differential equations: an introduction*, volume 92. Springer, 2015.
- [28] Jan S Hesthaven, Gianluigi Rozza, Benjamin Stamm, et al. *Certified reduced basis methods for parametrized partial differential equations*, volume 590. Springer, 2016.
- [29] Mario Ohlberger and Stephan Rave. Reduced basis methods: Success, limitations and future challenges. *arXiv preprint arXiv:1511.02021*, 2015.
- [30] Yasi Wang, Hongxun Yao, and Sicheng Zhao. Auto-encoder based dimensionality reduction. *Neurocomputing*, 184:232–242, 2016.
- [31] David Hartman and Lalit K Mestha. A deep learning framework for model reduction of dynamical systems. In *2017 IEEE Conference on Control Technology and Applications (CCTA)*, pages 1917–1922. IEEE, 2017.
- [32] Samuel E Otto and Clarence W Rowley. Linearly recurrent autoencoder networks for learning dynamics. *SIAM Journal on Applied Dynamical Systems*, 18(1):558–593, 2019.
- [33] Yann LeCun, Yoshua Bengio, and Geoffrey Hinton. Deep learning. *nature*, 521(7553):436–444, 2015.
- [34] Ian Goodfellow, Yoshua Bengio, and Aaron Courville. *Deep learning*. MIT press, 2016.
- [35] Kookjin Lee and Kevin T Carlberg. Model reduction of dynamical systems on nonlinear manifolds using deep convolutional autoencoders. *Journal of Computational Physics*, 404:108973, 2020.
- [36] Kaiming He, Xiangyu Zhang, Shaoqing Ren, and Jian Sun. Delving deep into rectifiers: Surpassing human-level performance on imagenet classification. In *Proceedings of the IEEE international conference on computer vision*, pages 1026–1034, 2015.

- [37] Adam Paszke, Sam Gross, Francisco Massa, Adam Lerer, James Bradbury, Gregory Chanan, Trevor Killeen, Zeming Lin, Natalia Gimelshein, Luca Antiga, et al. Pytorch: An imperative style, high-performance deep learning library. In *Advances in neural information processing systems*, pages 8026–8037, 2019.
- [38] Djork-Arné Clevert, Thomas Unterthiner, and Sepp Hochreiter. Fast and accurate deep network learning by exponential linear units (elus). *arXiv preprint arXiv:1511.07289*, 2015.
- [39] Diederik P Kingma and Jimmy Ba. Adam: A method for stochastic optimization. *arXiv preprint arXiv:1412.6980*, 2014.
- [40] Corinna Cortes and Vladimir Vapnik. Support-vector networks. *Machine learning*, 20(3):273–297, 1995.
- [41] Jason Weston, Chris Watkins, et al. Support vector machines for multi-class pattern recognition. In *Esann*, volume 99, pages 219–224, 1999.
- [42] F. Pedregosa, G. Varoquaux, A. Gramfort, V. Michel, B. Thirion, O. Grisel, M. Blondel, P. Prettenhofer, R. Weiss, V. Dubourg, J. Vanderplas, A. Passos, D. Cournapeau, M. Brucher, M. Perrot, and E. Duchesnay. Scikit-learn: Machine learning in Python. *Journal of Machine Learning Research*, 12:2825–2830, 2011.
- [43] Rich Caruana. Multitask learning. *Machine learning*, 28(1):41–75, 1997.
- [44] Michael Stein. Large sample properties of simulations using latin hypercube sampling. *Technometrics*, 29(2):143–151, 1987.
- [45] Martin Alnæs, Jan Blechta, Johan Hake, August Johansson, Benjamin Kehlet, Anders Logg, Chris Richardson, Johannes Ring, Marie E Rognes, and Garth N Wells. The fenics project version 1.5. *Archive of Numerical Software*, 3(100), 2015.